

Surface proteins modulate extracellular vesicle mediated inhibition of Aβ(1-42) aggregation

Downloaded from: https://research.chalmers.se, 2026-11-25 07:33 UTC

Citation for the original published paper (version of record):
Halipi, V., Daoutsali, G., Havemeister, F. et al (2026). Surface proteins modulate extracellular vesicle mediated inhibition of Aβ(1-42) aggregation. Protein Science, 35(12).
http://dx.doi.org/10.1002/pro.70849

N.B. When citing this work, cite the original published paper.

research.chalmers.se offers the possibility of retrieving research publications produced at Chalmers University of Technology. It covers all kind of research output: articles, dissertations, conference papers, reports etc. since 2004. research.chalmers.se is administrated and maintained by Chalmers Library

(article starts on next page)

Check for updates

Received: 30 April 2026 | Revised: 16 October 2026 | Accepted: 23 October 2026

DOI: 10.1002/pro.70849

RESEARCH ARTICLE

THE PROTEIN SOCIETY WILEY

Surface proteins modulate extracellular vesicle mediated inhibition of Aβ(1-42) aggregation

Vesa Halipi[1] | **Georgia Daoutsali**[1] | **Fritjof Havemeister**[1] | **Viktoria de Carvalho**[1] | **André Görgens**[2,3,4] | **Samir El Andaloussi**[2,3,4] | **Elin K. Esbjörner**[1]

[1]Division of Molecular Bioscience, Department of Life Sciences, Chalmers University of Technology, Gothenburg, Sweden

[2]Division of Biomolecular and Cellular Medicine, Department of Laboratory Medicine, Karolinska Institutet, Stockholm, Sweden

[3]Department of Cellular Therapy and Allogeneic Stem Cell Transplantation (CAST), Karolinska University Hospital, Huddinge, Sweden

[4]Karolinska ATMP Center, Karolinska Institutet, ANA Futura, Huddinge, Sweden

Correspondence
Elin K. Esbjörner, Division of Molecular Bioscience, Department of Life Sciences, Chalmers University of Technology, Gothenburg, Sweden.
Email: eline@chalmers.se

Funding information
Vetenskapsrådet, Grant/Award Numbers: 2016-03902, 2020-05303; Knut och Alice Wallenbergs Stiftelse, Grant/Award Numbers: 2019.0238, 2022.0134; Stiftelsen för Strategisk Forskning, Grant/Award Number: IRC15-0065

Review Editor: Jean Baum

Abstract

Aggregation of the amyloid-β (Aβ) peptide into amyloid oligomers and fibrils is a central pathogenic feature and therapeutic target in Alzheimer's disease (AD). Understanding the aggregation reaction and how it is modulated by the biological environment is therefore important. Cell-secreted extracellular vesicles (EVs) are emerging as modulators of Aβ aggregation, transport and toxicity. Here, we show that EVs from a variety of human and non-human cells have highly similar retarding effects on the rate of Aβ(1-42) fibril formation, suggesting that aggregation inhibition is a common EV feature. Furthermore, we examine how different EV biomolecular classes contribute to shape this effect. We show that enzymatic removal of surface-associated EV proteins significantly enhances their ability to inhibit aggregation. Similar, albeit considerably smaller, alterations were observed upon removal of cell surface protein-associated glycans. This suggests that EV-mediated inhibition of Aβ(1-42) aggregation may primarily be regulated by lipids and that surface proteins function to modulate this effect, through steric hindrance and/or direct interactions with Aβ(1-42) species. We further observed a minor but statistically robust enhancement of EV-mediated Aβ(1-42) aggregation inhibition upon removal of proteoglycans, suggesting that carbohydrates on the EV-surface also contribute to modulate their inhibitory effect. Altogether, these observations contribute mechanistic insight into the role of EVs as modulators of Aβ aggregation and highlight their possible contributions to maintenance of extracellular protein homeostasis.

KEYWORDS
Alzheimer's disease, amyloid kinetics, amyloid-β, EVs, extracellular vesicles, protein aggregation

1 | INTRODUCTION

Alzheimer's disease (AD) is a neurodegenerative disorder characterized by the aggregation of amyloid-beta (Aβ) peptides into insoluble fibrils that accumulate in the brain as extracellular plaque deposits (Tiwari et al., 2019). Preceding plaque formation, smaller soluble Aβ aggregates such as oligomers and short fibrils accumulate in both intracellular and extracellular locations of the brain (Takahashi et al., 2017) and their

This is an open access article under the terms of the Creative Commons Attribution License, which permits use, distribution and reproduction in any medium, provided the original work is properly cited.

© 2026 The Author(s). *Protein Science* published by Wiley Periodicals LLC on behalf of The Protein Society.

presence has been associated with neurotoxicity and neuronal degeneration in AD (Haass & Selkoe, 2007; Hampel et al., 2021; Lue et al., 1999; Scheltens et al., 2021). Antibody treatments targeting such Aβ aggregates have recently gained clinical approval due to their ability to moderately slow down early-stage disease progression (van Dyck et al., 2023). However, many Aβ-targeting drugs in clinical trials face challenges with target specificity and toxic side effects (Zhang et al., 2023), and their efficacy needs to be improved, emphasizing the importance of a better understanding of the mechanisms of Aβ aggregation and accumulation, as well as how these reactions are modulated by biological factors in the diseased brain.

Aβ is a proteolytic cleavage product of the membrane-bound amyloid precursor protein (APP) and exists as several isoforms of which the 42-residue variant Aβ(1-42) is known to be especially aggregation-prone and neurotoxic (Jarrett et al., 1993) whereas the shorter Aβ(1-40) variant is more abundant (Gravina et al., 1995). Biophysical studies of the self-assembly of various monomeric Aβ isoforms into amyloid fibrils have provided important insights into the molecular mechanisms of their fibrillation (Jan et al., 2011; Meisl et al., 2014; Scheltens et al., 2021; Selkoe & Hardy, 2016). Aβ(1-42) has been defined to follow a secondary nucleation-dominated process (Cohen et al., 2013) in which the auto-catalytic formation of new amyloid seeds on the surface of existing fibrils strongly dictates not only the rate of aggregate formation but also the generation of toxic oligomers (Cohen et al., 2013; Meisl, Yang, et al. 2016). Kinetic analysis of the modes of action of therapeutic anti-amyloid antibodies has furthermore indicated the significance of inhibiting the secondary nucleation step to achieve Aβ(1-42) aggregate suppression (Linse et al., 2020). On the other hand, it has been shown that fibrillation of Aβ(1-42) peptides carrying the aggregation-enhancing arctic mutation (E22G), which is associated with early onset AD, is instead dominated by fibril fragmentation (Bolognesi et al., 2014), suggesting that there is significant context-dependent modulation of the aggregation pathway and that this can affect both rates and morphological characteristics of ensuing aggregates, including their size.

Aβ aggregation is strongly modulated by the physicochemical conditions of the microenvironment (Cohen et al., 2015; Meisl, Yang, et al., 2016). Lipid membranes are critical in this context, both because of their omnipresence in subcellular and extracellular locations where Aβ peptides are abundant, including the endolysosomal system (Gouras et al., 2000) and synaptic cleft (Sokolow et al., 2012), and because of the links between dysregulation of lipid homeostasis in the brain and AD pathology (Di Paolo & Kim, 2011). Biophysical studies have shown that various brain-abundant membrane lipids, including cholesterol, sphingomyelin, ganglioside GM1, and phospholipids, can modulate various mechanistic steps in Aβ aggregation (Amaro et al., 2016; Habchi et al., 2018; Lindberg et al., 2017; Owen et al., 2018), resulting in both enhanced (Habchi et al., 2018; Lindberg et al., 2017; Owen et al., 2018) and inhibited (Amaro et al., 2016) fibrillation. The outcome of membrane-mediated regulation of Aβ aggregation is therefore likely dependent on the complexity and composition of the biological membrane (Sanguanini et al., 2020; Sasanian et al., 2025) and may, in a biological context, be further modulated by membrane-associated proteins and carbohydrates.

We recently demonstrated that cell-secreted, so-called extracellular vesicles (EVs) slow down Aβ(1-42) aggregation by interfering with the amyloid fibril elongation step and that their presence thereby diverts the aggregation outcome towards short fibrils (Halipi et al., 2024). EVs are high complexity cell-derived lipid vesicles that are increasingly recognized as important mediators of intercellular and inter-organ communication (Abels & Breakefield, 2016; van Niel et al., 2018), also in the brain (Basso & Bonetto, 2016). They have been implicated as carriers of misfolded and aggregated proteins in several neurodegenerative disorders (Hill, 2019), including as transporters of Aβ (Vandendriessche et al., 2020) as well as APP (van Niel et al., 2018; Welsh et al., 2024) in AD (Vandendriessche et al., 2020) and are suggested to contribute to prion-like propagation of protein aggregation pathologies (Vingtdeux et al., 2012).

Interestingly, we found that EVs from both neuroblastoma SH-SY5Y and non-neuronal human embryonic HEK293-T cells exhibited highly similar inhibitory effects on Aβ(1-42) aggregation despite the marked difference in cell source (Halipi et al., 2024), suggesting that the aggregation modulatory effect emanates from some common compositional feature of the EVs rather than brain-specific components. Moreover, these EV types were found to slow down fibril elongation (i.e., the addition of monomers to fibril ends), rather than affecting primary or secondary nucleation as seen in most biophysical studies with synthetic lipid membranes (Lindberg et al., 2017; Owen et al., 2018). This suggests that not only the lipid portion, but also the surface proteins and carbohydrates that are associated with EVs play an important role.

This study further dissects the origin of EV-mediated inhibitory effects on the aggregation of Aβ(1-42). We have examined EVs from a wider variety of cell sources but also used neuroblastoma-derived (SH-SY5Y) EVs to explore in more detail the role of EV surface proteins and protein-attached sugars (proteoglycans). These two biomolecular classes are, alongside lipids, important for EV functionalization (Jeppesen et al., 2014) affecting properties such as EV cell uptake and biodistribution (Cerezo-Magana et al., 2020; Christianson et al., 2013; Yanez-Mo et al., 2015). Proteoglycans, particularly those with heparan sulfate moieties, have, furthermore, been extensively studied in

1469896x, 2026, 12, Downloaded from https://onlinelibrary.wiley.com/doi/10.1002/pro.70849 by Statens Beredning, Wiley Online Library on [20/11/2026]. See the Terms and Conditions (https://onlinelibrary.wiley.com/terms-and-conditions) on Wiley Online Library for rules of use; OA articles are governed by the applicable Creative Commons License

the context of AD (van Horssen et al., 2003) and been shown to co-deposit with Aβ in plaques (Snow et al., 1994). We (Wesen et al., 2018) and others (Sandwall et al., 2010; Snow et al., 1990) have reported that proteoglycans, furthermore, promote Aβ cellular accumulation and regulate Aβ cytotoxicity.

This study extends our observation that EVs, regardless of cell source, slow down the in vitro aggregation of monomeric Aβ(1-42). Furthermore, we show that enzymatic digestion of EV surface proteins leads to a significant enhancement of this inhibitory effect, suggesting that these proteins have a marked and important regulatory role. Removal of surface-associated carbohydrates also contributes to the aggregation-modulatory effect of EVs, albeit to a lesser extent than proteins. Altogether, this study provides new insights into how EVs, through their surface composition, shape interaction with Aβ peptides and thus can tune aggregation outcomes. These findings extend our current understanding of how EVs may contribute to modulating Aβ pathology and hence their role in AD.

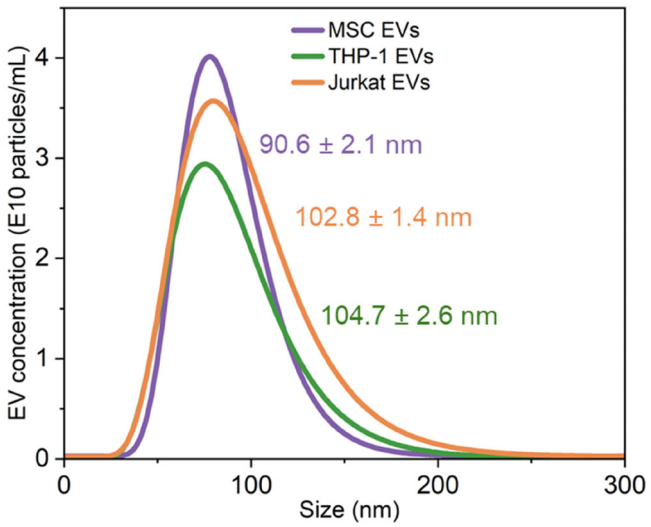

FIGURE 1 EV size distributions. Size distributions based on nanoparticle tracking (NTA) analysis for EVs derived from cord-blood derived MSC, THP-1, and Jurkat cells. The mean particle size in the different EV samples is shown as diameter ± standard deviation. The figure shows the distributions as nonlinear lognormal curves fitted to the raw NTA data, which can be found in Figure S1.

2 | RESULTS

2.1 | EVs from diverse cell sources slow down Aβ(1-42) aggregation

In previous work, we showed that EVs from both neuronal and non-neuronal cells inhibited Aβ(1-42) aggregation by an elongation inhibitory mechanism (Halipi et al., 2024). To explore the generality of this observation, we here examined additional EV sources, prepared from cultures of, respectively, umbilical cord-blood derived mesenchymal stromal (MSC) cells, human monocytic THP-1 cells, and Jurkat T-cells. MSC-derived EVs have been shown to exert immunomodulatory and neuroprotective effects in AD mouse models (Losurdo et al., 2020; Wang & Yang, 2021), whereas the THP-1 and Jurkat EVs were chosen because of their proposed links to neuroinflammation (Minter et al., 2016), microglia activation, and proinflammatory cytokine release (McGeer et al., 1987; Udan et al., 2008), conditions which are associated with AD. Prior to aggregation experiments, the EV samples were analyzed using Nanoparticle Tracking Analysis (NTA) to determine particle size and concentration (Figures 1 and S1), confirming a size distribution within the expected size range for small EVs (~50–200 nm [Jia et al., 2022]).

The effects of the three EV types on the kinetics of Aβ(1-42) fibril formation were analyzed using Thioflavin-T (ThT) fluorescence monitored kinetic assays (Figure 2a–c). This revealed that all EVs slowed down Aβ(1-42) aggregation in a concentration-dependent manner, consistent with our previous work (Halipi et al., 2024). An approximate three-fold increase in aggregation half-times (t_{half}) was observed at the highest EV concentration (7.2e9 particles/mL) tested (Figure 2d).

The aggregation kinetic curves were further analyzed by extracting lag-times (t_{lag}, defined as the reaction time for 10% of the total fibrillar content to form) and growth-times (t_{growth}, defined as the reaction time to increase the fibril content from 10% to 90% of the total fibrillar content) (Figure 2e,f). Although the magnitude and concentration-dependence of all these parameters were largely similar across the three EV types, two-way analysis of variance (ANOVA, Tables S1–S3) suggested statistically significant differences between EV types for all kinetic parameters (t_{half}, t_{lag}, and t_{growth}; $p < 0.01$, Tables S1–S3). This indicates subtle differences in their effects, likely relating to their compositions. Moreover, comparison of the t_{half} data in Figure 2d to our previously obtained data for human neuroblastoma derived SH-SY5Y and human embryonic kidney HEK293-T EVs (Halipi et al., 2024) shows that even though the inhibitory trend is highly consistent, this new panel of EVs is somewhat less effective, even after data has been compensated for slight variations in overall aggregation speed (Figure S2). Altogether, these observations support the hypothesis that EVs have a generic ability to slow down Aβ(1-42) aggregation but also highlight some variability suggesting that their exact biomolecular composition is also important.

In previous work, we established that EVs from SH-SY5Y and HEK293-T cells inhibit Aβ(1-42) fibril elongation, based on kinetic modeling of seeded and unseeded aggregation data and the observation that

1469896x, 2026, 12, Downloaded from https://onlinelibrary.wiley.com/doi/10.1002/pro.70849 by Statens Beredning, Wiley Online Library on [20/11/2026]. See the Terms and Conditions (https://onlinelibrary.wiley.com/terms-and-conditions) on Wiley Online Library for rules of use; OA articles are governed by the applicable Creative Commons License

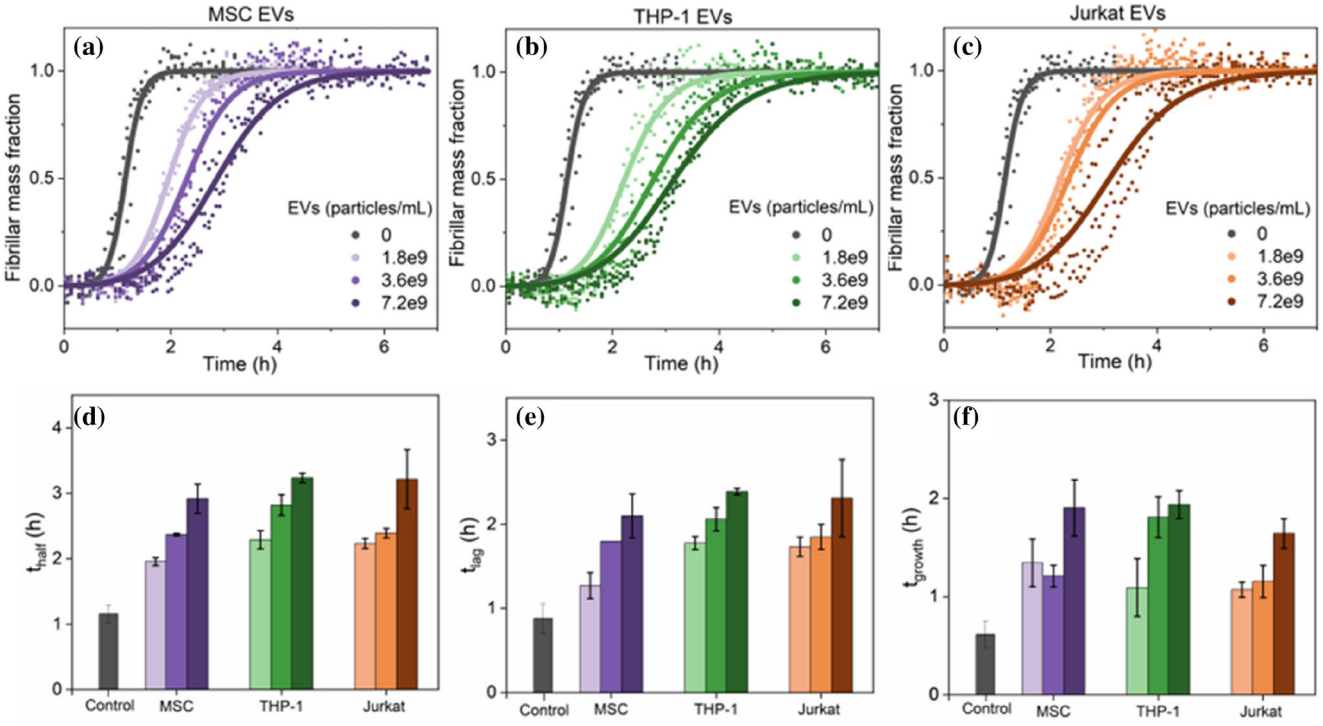

FIGURE 2 Aβ(1-42) aggregation kinetics in the presence of cord-blood derived MSC, THP-1, and Jurkat EVs. (a–c) Normalized ThT fluorescence assay over time showing Aβ(1-42) aggregation (2 μM) in absence or presence of indicated EV concentrations isolated from (a) umbilical cord-blood derived MSCs, (b) THP-1 cells, and (c) Jurkat cells. The dotted lines are experimental data points, and the solid lines show fittings of the experimental data using a multi-step secondary nucleation dominated model for amyloid formation setting the combined rate constants for elongation and secondary nucleation (k_+k_2) as a free parameter, as described in the main text and in Section 4. (d–f) Reaction half-times (t_{half}) (d), lag-times (t_{lag}) (e), and growth-times (t_{growth}) (f). The error bars represent the standard deviation ($n = 3$). Statistics: Two-way ANOVA for factors EV type and concentration; see full ANOVA results in Tables S1–S3.

EVs reduced fibril length (Halipi et al., 2024). Here, we further analyzed the aggregation kinetics by fitting a multi-step secondary nucleation model to the kinetic data, using the online Amylofit tool (Meisl, Kirkegaard, et al., 2016) as described in Section 4. The fitted curves are shown as solid lines in Figures 2a–c and S3a–c. We used a procedure with sequential fitting where one of the two combined rate constants in the model (k_+k_n which is the product of elongation and primary nucleation rates, or k_+k_2 which is the product of elongation and secondary nucleation rates (k_+k_2)) were kept constant to explore how well the inhibitory effect of EVs could be explained by variation in the other (free) rate constant (Sasanian et al., 2025). This identified inhibition of secondary aggregation pathways (k_+k_2) as the dominant aggregation-retarding effect, evident both from visual inspection of the fit (Figure 2a–c vs. Figure S3a–c) and comparison of mean residual errors (MRE) (Tables S4–S6). Although it is not possible to decouple effects on secondary nucleation and elongation using this data analysis approach, the change in shape of the kinetic curves with extensions of both t_{lag} and t_{growth} (Figure 2e,f) is highly similar to our previous work (Halipi et al., 2024) and in line with the expected behavior of elongation inhibitors (Munke et al., 2017). Furthermore, the conclusion is supported by observations that EVs from the MSC, THP-1 and Jurkat cells shortened Aβ(1-42) fibrils (see below).

Having established that EVs of different cellular origins share a common mechanistic ability to slow down Aβ(1-42) fibril formation, we proceeded to analyze Aβ(1-42) fibril morphology using Atomic Force Microscopy (AFM). Figures 3a–d and S4 show representative images of mica-deposited, dried, Aβ(1-42) fibrils taken at the endpoints of kinetic experiments. The images confirm the formation of fibrils both in the absence of EVs (buffer) and in the presence of EVs at a concentration of 7.2e9 particles/mL (the highest concentration tested), consistent with the observed enhancement of ThT fluorescence (Figure 2). In addition, small spherical particles appeared in EV-containing samples (Figure 3b–d) suggesting possible formation of oligomers. This was not observed in our previous work (Halipi et al., 2024). However, we also noted that the background in EV-containing samples was coarser than for Aβ(1-42) alone, suggesting that EVs may have adsorbed and ruptured on the mica surface during drying (white square in Figure 3d and Figure S5).

The AFM images were used to estimate fibril lengths (Figure 3e) and cross-sectional heights

1469896x, 2026, 12, Downloaded from https://onlinelibrary.wiley.com/doi/10.1002/pro.70849 by Statens Beredning, Wiley Online Library on [20/11/2026]. See the Terms and Conditions (https://onlinelibrary.wiley.com/terms-and-conditions) on Wiley Online Library for rules of use; OA articles are governed by the applicable Creative Commons License

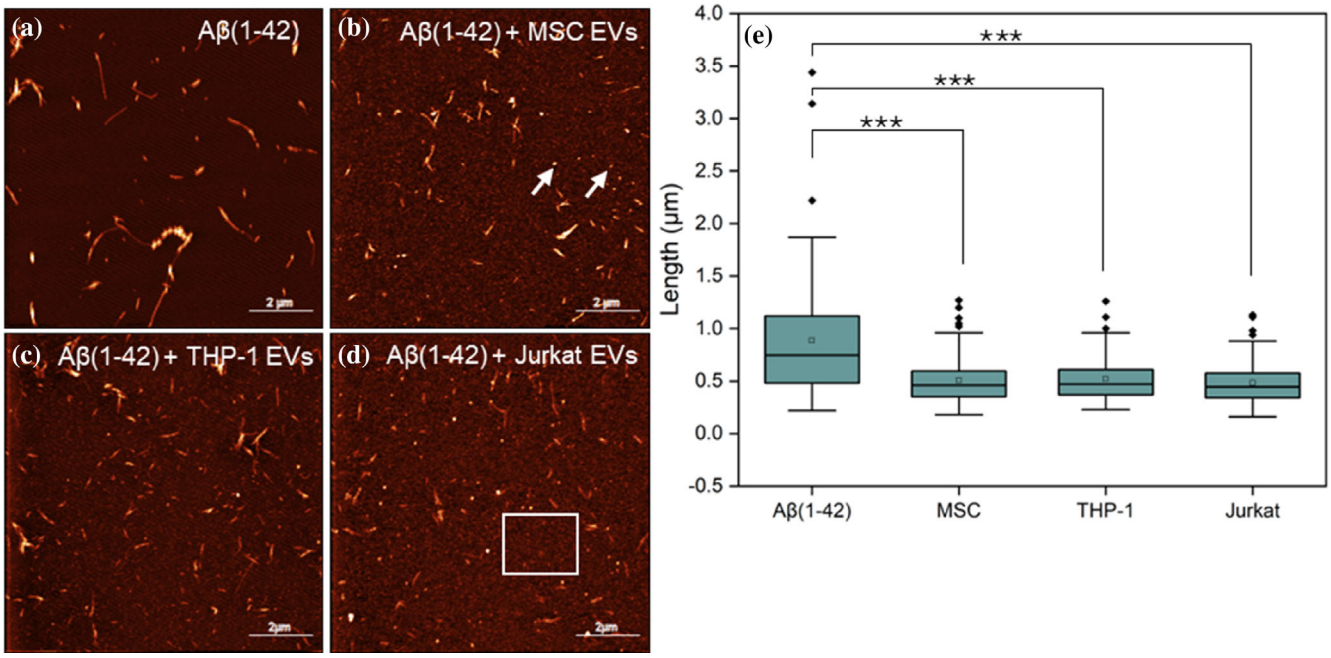

FIGURE 3 Morphological analysis of Aβ(1-42) fibrils formed in absence and presence of EVs. (a–d) Representative AFM images of Aβ(1-42) aggregation (2 μM) in absence (a) or presence of EVs from (b) umbilical cord-blood derived MSCs, (**c**) THP-1 cells, and (d) Jurkat cells. Scale bars = 2 μm. White arrows indicate smaller aggregate species in EV samples, and the white square marks the altered surface background in presence of EVs. (e) Analysis of fibril length based on AFM images (see Section 4) of Aβ(1-42) fibrils (mean ± standard deviation, $n = 100$ fibrils from 11 images for the Aβ(1-42) + THP-1 EVs condition and from 10 images for the other conditions, *** denotes $p < 0.001$, by one-way ANOVA and Post hoc Bonferroni-corrected means comparison tests) formed in absence and presence of the indicated EVs. The EV concentration was 7.2e9 particles/mL in all conditions containing EVs. Box plots represent the interquartile range (25–75th percentile), mean values are presented as squares, median values as horizontal lines. Whiskers indicate values within 1.5× the interquartile range and black diamonds show outliers.

(Figure S6). While the Aβ(1-42) fibrils formed in the presence of EVs showed small variations in cross-sectional heights compared to fibrils formed in buffer, fibril lengths were significantly altered. The mean lengths of fibrils were 506 ± 23 nm for fibrils formed in the presence of MSC-derived EVs, 518 ± 20 nm in the presence of THP-1-derived EVs, and 481 ± 20 nm in the presence of Jurkat-derived EVs, compared to 886 ± 57 nm for Aβ(1-42) fibrils formed in buffer. This corresponds to a fibril length reduction of ca 45% and is a clearly significant effect (one-way ANOVA, $p < 0.001$), consistent with our previous reports where EVs were shown to reduce fibril length by 40% (Halipi et al., 2024). Small differences in mean fibril lengths were observed among the different samples, but these were not statistically significant (post hoc Bonferroni-corrected means comparison $p > 0.99$). Notably, the observation of EVs reducing fibril length supports the above conclusion of interference with the elongation step, as inhibition of secondary nucleation (which would be the other possible effect agreeing with the fitting of kinetic data) would instead significantly limit the number of aggregates formed and hence drive generation of longer fibrils under conditions where the total peptide concentration is constant. Altogether, by extending kinetic and morphological analysis of Aβ(1-42) to a broader panel of EVs, this study supports the idea that EVs, independently of their cellular origin, slow down Aβ(1-42) aggregation by a common mechanism.

2.2 | Surface proteins modulate the aggregation-inhibitory effect of EVs

EVs have a diverse surface proteome consisting of both integral and peripheral membrane proteins, and other adsorbed proteins (Hallal et al., 2022). The membrane-associated protein content can amount to up to 50% (w/w) or more of the EV membrane (Osteikoetxea et al., 2015) and may, to a large extent, cover the EV surface (Hallal et al., 2022). We therefore hypothesized that they must contribute to modulate Aβ(1-42) aggregation. To test this idea, we used EVs from SH-SY5Y neuroblastoma cells, which are common neurodegenerative disease cell models (Agholme et al., 2010; Xicoy et al., 2017) and established a protocol to enzymatically digest their surface proteins using trypsin. The trypsin-treated EVs were separated from trypsin and released protein fragments using

14698896x, 2026, 12, Downloaded from https://onlinelibrary.wiley.com/doi/10.1002/pro.70849 by Statens Beredning, Wiley Online Library on [20/11/2026]. See the Terms and Conditions (https://onlinelibrary.wiley.com/terms-and-conditions) on Wiley Online Library for rules of use; OA articles are governed by the applicable Creative Commons License

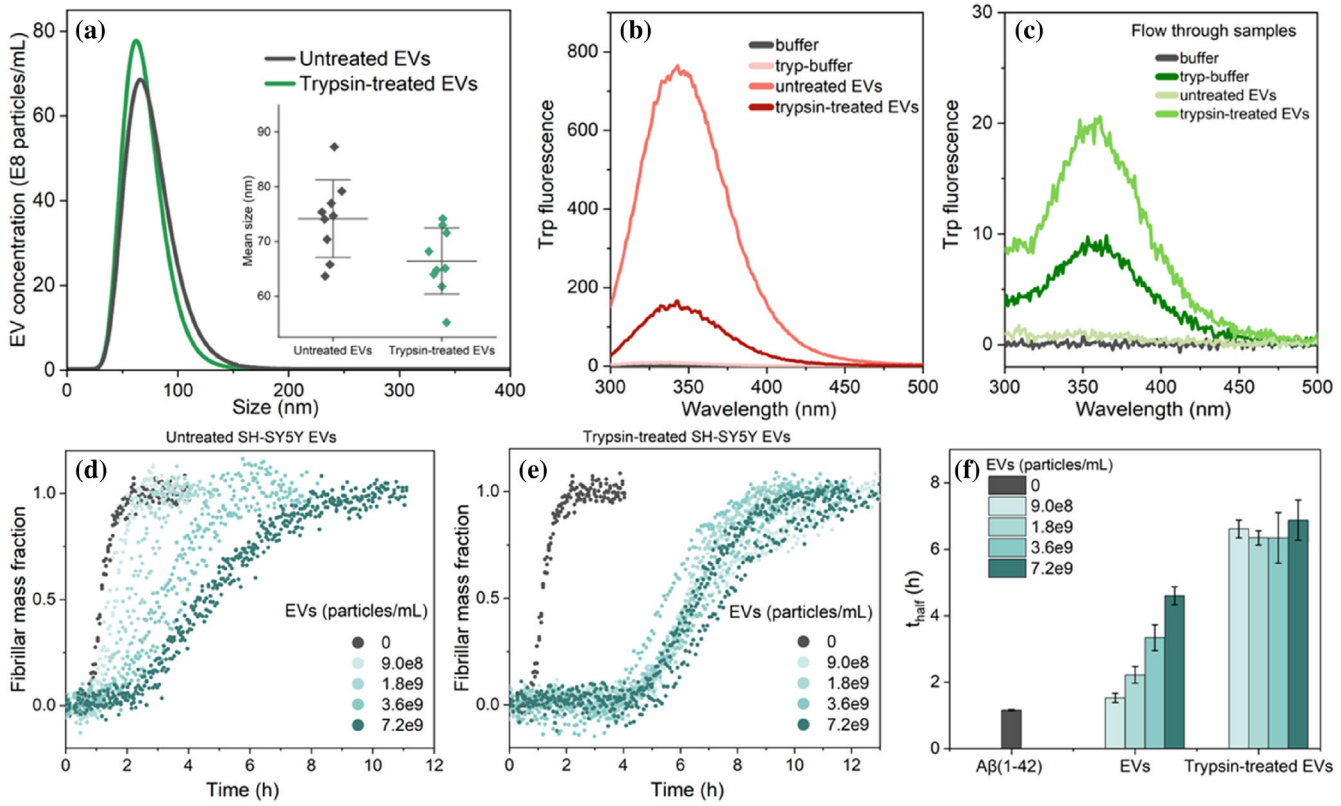

FIGURE 4 Characterization of EV surface protein digestion after trypsin-treatment and their effect on Aβ(1-42) aggregation kinetics. (a) Size distributions and concentrations of SH-SY5Y EVs, untreated EVs (black) and trypsin-treated EVs (green) as determined by NTA. Curves show one representative NTA measurements while distribution plots show mean size of EVs ± SD per group ($n = 9$). (b and c) Tryptophan (and tyrosine) fluorescence of EV samples (b) and flow through (c) after trypsin-treatment and removal of peptide fragments and trypsin with ultrafiltration (see Section 4). Note that the absolute intensities in (b) and (c) cannot be compared because of the substantial (>20-fold) dilution during ultrafiltration. (d and e) Normalized aggregation kinetic curves of 2 μM Aβ(1-42) in absence or presence of untreated (d) vs. trypsin-treated (e) SH-SY5Y EVs on Aβ(1-42) aggregation kinetics. (f) Reaction half-times (t_{half}) as a function of EV concentration, derived from the data in (d and ed).

ultrafiltration. The removal was first verified by NTA, showing that trypsin-treated EVs had ∼8 nm smaller diameter than control EVs (Figure 4a, Table S7). This corresponds to a ∼4 nm thinning of the EV leaflet and is comparable to size reductions following enzymatic protein digestion reported by others (Choi et al., 2020; Shtam et al., 2018; Silva et al., 2025; Skliar et al., 2018). Importantly, the trypsin treatment did not significantly reduce EV concentration (Figure S7), suggesting that their membranes remained intact.

To further confirm that the trypsin treatment and subsequent trypsin removal was effective, we analyzed the intrinsic protein fluorescence emanating from tryptophan and tyrosine in the ultrafiltrated EV samples (Figure 4b) as well as the flow-through (Figure 4c) using fluorescence spectroscopy. Control experiments where trypsin solutions with the same concentration used for digestion were ultrafiltrated in absence of EVs verified that trypsin was effectively removed (Figure S8). Next, we examined EV samples and found that the level of intrinsic fluorescence was ∼80% lower in the trypsin-treated EV sample compared to the untreated EV control (Figure 4b). Moreover, the fluorescence spectra had emission maxima around 340 nm, which is consistent with the spectral signature of tryptophan in folded or membrane-associated proteins (Lakowicz, 1988). Furthermore, the flow-through of the ultrafiltrated trypsin-treated EV sample showed substantial fluorescence in combination with a significant spectral red-shift, consistent with the presence of unfolded fragments with solvent-exposed tryptophan residues in this fraction, whereas the corresponding flow-through for non-trypsinized EVs showed negligible fluorescence (Figure 4c).

Using ThT kinetic assays, we found that trypsin-treated EVs had a markedly stronger inhibitory effect on Aβ(1-42) aggregation than untreated EVs. They also significantly altered the shapes of the kinetic curves and, as a consequence, the aggregation kinetic parameters (Figures 4d–f and S9), whereas the reduction in fibril length was comparable between trypsin-treated (Figure S10) and untreated EVs (Figure 3). When used at the same particle concentration as untreated EVs, trypsinized EVs produced a saturating inhibitory effect.

1469896x, 2026, 12, Downloaded from https://onlinelibrary.wiley.com/doi/10.1002/pro.70049 by Statens Beredning, Wiley Online Library on [20/11/2026]. See the Terms and Conditions (https://onlinelibrary.wiley.com/terms-and-conditions) on Wiley Online Library for rules of use; OA articles are governed by the applicable Creative Commons License

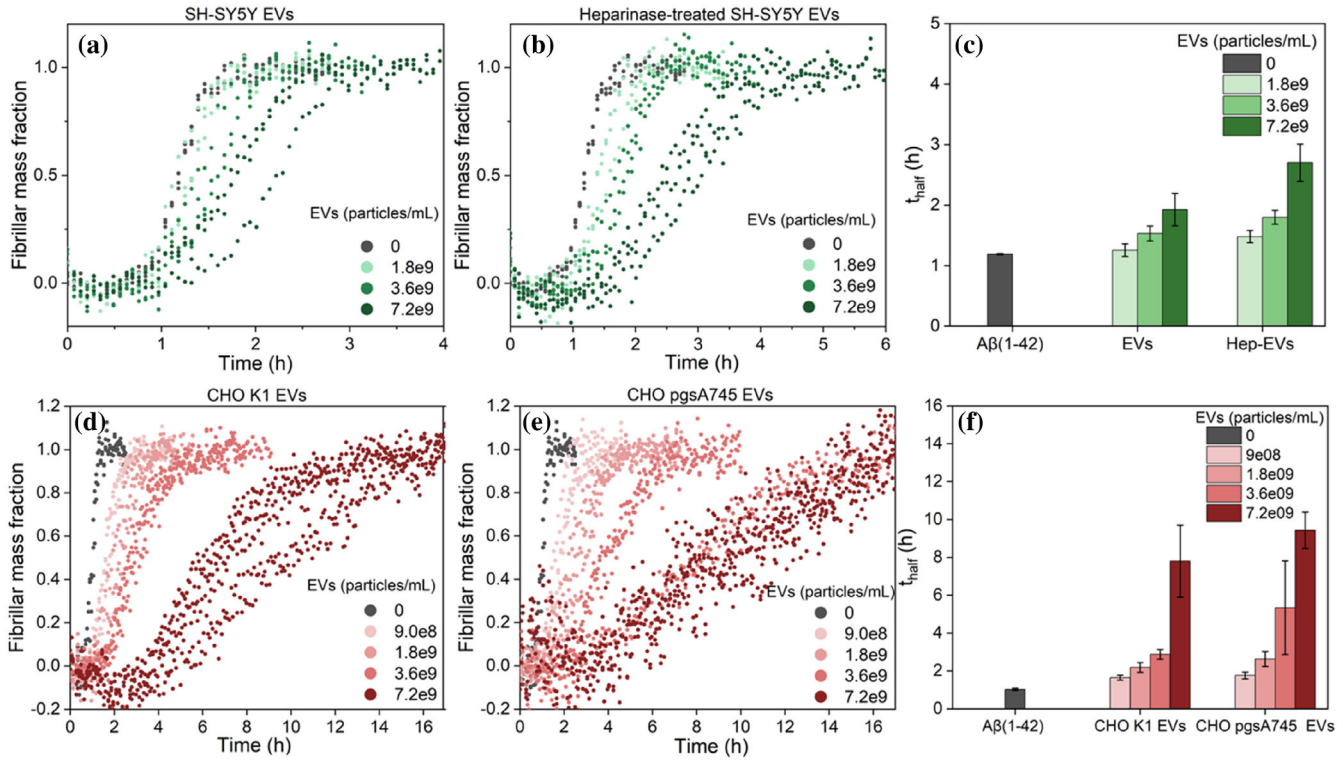

FIGURE 5 The effect of EV proteoglycans on Aβ(1-42) aggregation kinetics by glycosaminoglycan modified vs non-modified SH-SY5Y and CHO EVs. (a and b) Normalized Aβ(1-42) aggregation kinetic curves showing the effect SH-SY5Y vs HSPG-lacking SH-SY5Y EVs. (c) Half-times extracted from (a and b). (d and e) Normalized Aβ(1-42) aggregation kinetic curves showing the effect of EVs from wildtype CHO-K1 cells and pgsA-745 mutant CHO cells. (f) Half-times extracted from (d and e). Statistics: Two-way ANOVA for factors EV type and concentration; see full ANOVA results in Tables S9–S11.

We therefore also examined a lower concentration range, where aggregation kinetic data, including half-times, show that dose dependence was restored (Figure S11). Altogether this suggests that trypsinized EVs have a more potent inhibitory effect compared to their untreated counterparts. We excluded the possibility that residual trypsin would cause this enhanced inhibition by simply digesting Aβ(1–42) monomers by repeating the kinetic experiments using the retentate of an ultrafiltrated trypsin-only sample. This had no effect on Aβ(1-42) aggregation (Figure S12). Thus, it appears that EV surface proteins contribute to modulate Aβ(1-42) aggregation and that their removal substantially enhances inhibition, possibly because Aβ(1-42) species can more readily interact with EV membrane lipids.

2.3 | EV-associated proteoglycans have minor effect on Aβ(1-42) aggregation

Proteolytic digestions of EV surface proteins also remove protein-attached carbohydrates (glycosaminoglycans, GAGs). To explore whether EV cell-surface carbohydrates are important in Aβ(1-42) aggregation, we used two complementary experimental approaches. First, we compared the aggregation inhibitory effect of heparinase II treated and normal SH-SY5Y derived EVs (Figure 5a,b). They had largely similar efficacy, but produced subtle differences to aggregation kinetic parameters, especially at the highest EV concentration tested (Figures 5c and S13a,b, two-way ANOVA; $p < 0.005$). Since sugars have no specific absorption or emission properties it was not straightforward to quantify the extent of their removal. NTA-based comparison of EV size revealed no consistent differences between heparinase-treated and untreated EVs (Table S8), which is not unexpected given that other surface glycans, including chondroitin sulfate and glycans associated with glycoproteins and glycolipids, remain unaffected by heparinase treatment. We therefore complemented this approach by comparing EVs from two Chinese hamster ovary (CHO) cell lines with respectively normal (CHO-K1) and deficient (CHO-pgsA-745) GAG expression (Esko et al., 1985). CHO-pgsA-745 cells lack xylosyltransferase which is responsible for the initial sugar transfer in GAG synthesis and this cell line therefore completely lacks protein-bound sulfated sugars (Esko et al., 1985) resulting in a lower zeta potential (Amand et al., 2012). The EVs from the GAG-deficient CHO-pgsA-745 cells were approximately 7 nm in diameter smaller than EVs from wildtype

1469896x, 2026, 12, Downloaded from https://onlinelibrary.wiley.com/doi/10.1002/pro.70849 by Statens Beredning, Wiley Online Library on [20/11/2026]. See the Terms and Conditions (https://onlinelibrary.wiley.com/terms-and-conditions) on Wiley Online Library for rules of use; OA articles are governed by the applicable Creative Commons License

CHO-K1 cells (Table S8), consistent with a contribution of surface-associated GAGs to EV hydrodynamic size. Aggregation kinetics experiments showed that EVs from both these cell types slowed down Aβ(1-42) aggregation (Figure 5d,e) and reduced fibril lengths (Figure S10), representing yet an example of EVs with inhibitory effect. The Aβ(1-42) kinetic curves obtained in the presence of GAG-deficient EVs had slightly longer t_{half}, t_{growth}, and t_{lag} (Figures 5f and S13c,d; two-way ANOVA; $p < 0.05$). Altogether, this suggests that proteoglycans contribute to modulate EV-mediated inhibition of Aβ(1-42) aggregation, albeit to a much lesser extent than EV surface proteins.

3 | DISCUSSION

Despite that Aβ aggregation and senile plaque deposition are the most well-recognized pathological features of Alzheimer's disease (AD), key mechanistic and molecular understanding of the drivers and propagators of this pathology remains missing. This presents a pressing knowledge gap and bottleneck in drug discovery. This study explores EVs as modulators of the Aβ(1-42) aggregation pathway. The central conclusion of the work is that EVs, irrespective of the lineage, have highly similar effects slowing down Aβ(1-42) aggregation. This points toward an aggregation-reducing mechanism that is largely conferred by common EV properties rather than by specific EV ligands.

EVs have been implicated as versatile mediators of the pathology of AD (Da Conceicao et al., 2025; Gabrielli et al., 2022; Vingtdeux et al., 2012) and other neurodegenerative diseases (Hill, 2019) through actions involving, for example, transport of protein aggregates (Rajendran et al., 2006) or plaque clearance (Elia et al., 2019). EVs have also been reported to impact cognitive function (Wang & Yang, 2021). This study focuses directly on EV-Aβ(1-42) interactions, which may, for example, occur in the interstitial space of the brain, where animal studies indicate that EV concentrations increase with the emergence of plaque pathology (Pait et al., 2024). Our study shows that EVs from three different cell lines (MSC, THP-1, and Jurkat) slow down Aβ(1-42) aggregation. The kinetic profiles showed high similarity to those in a previous study of SH-SY5Y and HEK293-T derived EVs, in which seeded aggregation experiments demonstrated that the inhibitory effect was retained under elongation-dominated conditions (Halipi et al., 2024). This, together with data fitting and the observation that the MSC, THP-1, and Jurkat derived EVs also induced the formation of shorter Aβ(1-42) fibrils, supports a shared mechanism of EV-mediated inhibition of fibril elongation across EVs from different cell sources. Short fibrils, akin to oligomers, are diffusible and have been generally associated with neurotoxicity (Xue et al., 2009; Zhang et al., 2020). We have thus previously suggested that EVs have the capacity to alter the Aβ aggregation landscape in both protective (aggregation-suppressive) and putatively detrimental ways.

The observation that EVs have generic rather than specific abilities to slow down Aβ(1-42) aggregation is interesting because a more common notion in the EV field is that EVs (or at least a subset of EVs) rather have highly specialized functions that are tied to their exact biological compositions. Our data highlight that, in the context of protein aggregation, it is rather commonalities in biophysical and biochemical features that are important and a key focus of this study has therefore been to identify and understand the relative contribution of different biomolecular classes. Nevertheless, we observed modes of differences in the potency of EVs from different cell sources to inhibit Aβ(1-42) aggregation, suggesting that differences in EV composition, including the surface proteome, glycan profile, and lipid composition, may modulate their interactions with monomeric and fibrillar Aβ(1-42), thereby contributing to variations in inhibitory activity between EV types.

The EV surface is normally densely populated by both membrane-incorporated and more loosely associated proteins. These proteins participate in targeting, cell interactions, cell uptake, and cell signaling (Wang et al., 2025), contributing to EV specialization and functionalization. Some are broadly shared across EV types and often linked to EV biogenesis and release, whereas other proteins are more specialized, reflecting their cellular origin and microenvironment (Amin et al., 2024). This study shows that generic (trypsin-mediated) removal of the surface-associated proteins on EVs enhances their inhibitory effect on Aβ(1-42) aggregation. This could suggest that the lipid bilayer, which likely becomes more exposed when surface proteins are digested, has a particularly potent inhibitory effect and that EV proteins in fact act to modulate or even hinder inhibitory EV-Aβ(1-42) interactions. This could be due to steric hindrance or shielding constraints; notably, our study shows that trypsination leads to an approximate 4 nm thinning of the outer EV leaflet, supporting that EVs have a dense protein layer limiting direct access to their membrane lipids. Interestingly, a proteomic study on EVs isolated from interstitial fluid of live mice reported that EV concentrations increase, but their protein levels decrease with Aβ plaque formation (Pait et al., 2024). This could result in that brain-derived EVs gradually lose their inhibitory potency with the progression of AD pathology and suggests that EVs may contribute to uphold extracellular proteostasis.

Following trypsin-mediated protein removal, the EV surface can, to approximation, be considered lipid-dominated. EV membranes are typically enriched in lipids such as cholesterol (Chol), sphingomyelin (SM), and phosphatidylserine (Ghadami & Dellinger, 2023;

1469896x, 2026, 12, Downloaded from https://onlinelibrary.wiley.com/doi/10.1002/pro.70849 by Statens Beredning, Wiley Online Library on [20/11/2026]. See the Terms and Conditions (https://onlinelibrary.wiley.com/terms-and-conditions) on Wiley Online Library for rules of use; OA articles are governed by the applicable Creative Commons License

Skotland et al., 2020), but also various gangliosides (He et al., 2022). Brain-relevant lipids such as Chol, glycolipids, and SM, which are, alongside phospholipids, common in EVs, have been studied by us and others in the context of Aβ(1-42) aggregation and reported to either catalyze or inhibit Aβ(1-42) fibril formation (Amaro et al., 2016; Calamai & Pavone, 2013; Habchi et al., 2018; Lindberg et al., 2017; Owen et al., 2018). Studies investigating the effects of mixed lipid membranes, which are arguably more relevant in the context of EVs, report a variety of outcomes, ranging from findings suggesting that more complex membranes balance opposing effects of individual lipids on Aβ(1-42) aggregation (Sanguanini et al., 2020) to reports of either accelerated or inhibited aggregation depending on membrane composition (Banerjee et al., 2021; Baumann et al., 2023). We have recently shown that synthetic, protein-free, lipid vesicles with SM/Chol/GM1-content can both catalyze and inhibit Aβ(1-42) aggregation depending on their exact lipid compositions (Sasanian et al., 2025). Furthermore, we showed that under lipid-raft promoting compositions, the synthetic vesicles always inhibited Aβ(1-42) aggregation. This is interesting given that EV membranes are generally reported to be more rigid than typical plasma cell membranes (Laulagnier et al., 2004; Parolini et al., 2009) and furthermore relevant because Aβ is known to bind to clusters of glycosphingolipids (Ariga et al., 2008; Yanagisawa et al., 1995), which are also enriched on EV surfaces (Yuyama et al., 2014). However, given the complexity of EV membranes and the fact that comprehensive lipidomic data on EVs remain limited, it is challenging to fully recapitulate their key features in simplified synthetic lipid models. Future studies combining EV lipidomic profiling with the extraction of EV lipids and their reconstitution into synthetic vesicles could help better establish how native EV lipid compositions contribute to Aβ(1-42) self-assembly.

Notably, the aggregation kinetics we observe for Aβ(1-42) in the presence of trypsin-treated EVs have a conspicuous extended lag phase, similar to what we report for GM1-mediated inhibition (Sasanian et al., 2025) and explain by primary nucleation inhibition. This contrasts with the identification of EVs as inhibitors of fibril elongation in this and our previous (Halipi et al., 2024) work and suggests that EV surface proteins modulate not only the rate but also their mechanism of inhibition.

Lastly, this study also explores the possible contribution of protein-attached EV glycans to Aβ(1-42) aggregation showing that they have extremely modest effects. This is interesting given the reported roles of proteoglycans in Aβ uptake and accumulation (Sandwall et al., 2010; Wesen et al., 2018) and reports that soluble heparin can modulate Aβ self-assembly (Radko et al., 2018). Glycans are also considered as generally important for the function of EVs (Williams et al., 2018).

In conclusion, this study shows that EVs from a variety of cell sources have common and potent abilities to inhibit Aβ(1-42) aggregation, expanding our previous findings (Halipi et al., 2024). Moreover, we show that EV surface proteins, and to a lesser extent carbohydrates, are important modulators of the aggregation-inhibitory effect that we propose originates from Aβ(1-42) interactions with the EV lipid interface. Altogether, this work provides a more detailed understanding for the role of EVs in AD pathology and pinpoints them as important aggregation regulators and putative contributors to protein homeostasis, acting in the interstitial space.

4 | MATERIALS AND METHODS

4.1 | Cell culture and cell lines

SH-SY5Y cells were cultured in 1:1 medium of MEM + GlutaMAX and F-12 Nut Mix (Gibco, USA) supplemented with 10% FBS and 1% non-essential amino acids (Gibco, USA). CHO cells were cultured in DMEM (Gibco, USA) supplemented with 10% FBS. Cell line authentication based on genotyping was performed according to ANSI/ATCC standard ASN-0002 (Eurofins Genomics) for SH-SY5Y cells. SH-SY5Y and CHO cells were cultured in T75 flasks (Thermo Scientific) at 37°C and 5% CO_2 until 70% confluence, after which cell medium (CM) was exchanged to 1:1 medium of MEM + GlutaMAX and F-12 Nut Mix without FBS for SH-SY5Y and DMEM without FBS for CHO cells for 48 h. CM was collected for EV isolation.

Umbilical cord-blood derived mesenchymal stromal cells (MSC) were cultured in MEM-α modification medium (containing L-glutamine; Thermo Fisher Scientific) supplemented with basic fibroblast growth factor (5 ng/mL; Sigma–Aldrich) and 10% FBS and 1X antibiotic-antimycotic (Thermo Fisher Scientific) as described previously (Hagey et al., 2023). THP-1 and Jurkat cells were cultured in RPMI-1640 medium containing GlutaMAX-I and 25 mM HEPES (Invitrogen) supplemented with 10% FBS and 1× antibiotic-antimycotic. Cells were cultured at 37°C and 5% CO_2 and regularly tested for the presence of mycoplasma. The CM was changed to optiMEM (Invitrogen) without FBS for 48 h before collection of CM for EV isolation.

4.2 | EV isolation

EVs were collected as previously described (Halipi et al., 2024). CM was centrifuged at low speed (2000 g) for 20 min to remove larger particles and cell debris and subsequently filtered through a 0.22 μm pore size (VWR) membrane. This was followed by ultrafiltration with Amicon Ultra-15 10 kDa (Millipore) spin filters at

1469896x, 2026, 12, Downloaded from https://onlinelibrary.wiley.com/doi/10.1002/pro.70849 by Statens Beredning, Wiley Online Library on [20/11/2026]. See the Terms and Conditions (https://onlinelibrary.wiley.com/terms-and-conditions) on Wiley Online Library for rules of use; OA articles are governed by the applicable Creative Commons License

5000 *g* for 2 h. The collector tube was emptied, and Dulbecco's phosphate-buffered saline (DPBS) (ThermoFisher Scientific) was added prior to a second centrifugation at the same speed. SH-SY5Y EVs were stored in DPBS at 4°C and used within 2 days for all experiments. All samples were stored on ice during the isolation process. Isolation of EVs from umbilical cord-blood derived mesenchymal stromal cells (MSC), THP-1 and Jurkat cells was performed by centrifuging CM at low speed (500 *g*) for 5 min followed by a 2000 *g* spin for 10 min to remove larger particles and cell debris, after which the pre-cleared cell culture supernatant was filtered through a 0.22 μm bottle top vacuum filter (Corning). EVs were first prepared by tangential flow filtration (TFF) using a KR2i TFF system (SpectrumLabs) equipped with modified polyethersulfone (mPES) hollow fiber filters with 300 kDa membrane pore size (MidiKros, 370 cm^2 surface area, SpectrumLabs) at a flow rate of 100 mL/min (transmembrane pressure at 3.0 psi and shear rate at 3700 s^{-1}) as described previously (Corso et al., 2017). Amicon Ultra-0.5 10 kDa MWCO spin-filters (Millipore) were used to concentrate the sample to a final volume of 100 μL. These EVs were stored in DPBS buffer containing 0.2% albumin, 25 mM HEPES and 25 mM Trehalose (PBS-HAT) (Gorgens et al., 2022). The EVs were stored at −80°C upon delivery and thawed on ice directly prior to all experiments.

4.3 | EV trypsin treatment

EVs were treated with trypsin (Gibco) at a concentration of 1.25 mg/mL at 37°C for 30 min. DPBS was added to control EV samples not subjected to trypsin treatment, and these were also incubated at 37°C for 30 min. After the incubation, samples were diluted in DPBS, introduced to Amicon Ultra-15 30 kDa (Millipore) spin filters, and centrifuged at 6400 rpm with several DPBS washes to remove trypsin and peptide fragments. EVs were collected, stored at 4°C, and used within 2 days for all experiments.

4.4 | Heparinase treatment

We utilized a heparinase II (25 Units/mL) from Flavobacterium heparinum (Sigma–Aldrich), which was diluted in DPBS to a concentration of 2.5 U/mL, aliquoted and stored at −20°C until further use. SH-SY5Y EVs were treated with 5, 10, or 20 mU/mL for 2 h or with 20 mU/mL for 3, 6, and 24 h. Only data from the 20mU/mL treatment for 24 h are shown. EV samples treated with heparinase were kept at 4°C and used within 2 days for aggregation experiments. No further steps were taken to remove the heparinase or any heparan sulfate (HS) fragments.

4.5 | Nanoparticle tracking analysis (NTA)

Mean size (diameter) and concentration of EVs were determined by NTA using a NanoSight LM14 instrument with NTA 3.3 software (Malvern Instruments). Five consecutive 60 s videos were recorded per sample in light scatter mode, screen gain 5.0, and camera setting of 14. All EV samples were diluted in 0.22 μm filtered DPBS prior to NTA measurements. Software settings were kept constant for all measurements to obtain comparable results. A detection threshold of 2 for SH-SY5Y or 3 for umbilical cord-blood MSC, THP-1, Jurkat EVs, and CHO EVs was used, respectively.

4.6 | Fluorescence spectroscopy measurements

Extracellular vesicles were isolated from cultured cells and subjected to trypsin treatment as described above. Intrinsic fluorescence from aromatic amino acids (primarily tryptophan and tyrosine) was recorded for untreated and trypsin-treated EV samples using a Cary Eclipse fluorescence spectrophotometer (Agilent). Samples were measured in a 10 mm path length quartz cuvette. Emission spectra were collected from 300 to 500 nm with an excitation wavelength of 280 nm. Both excitation and emission slit widths were set to 5 nm. Spectra were acquired at a scan rate of 600 nm/min using a photomultiplier tube (PMT) voltage of 600 V.

4.7 | Aβ(1-42) expression and purification

Recombinant Aβ(1-42) was expressed overnight in E. coli (BL21) as a fusion protein with an NT* solubility tag (Abelein et al., 2020). In brief, bacterial cells were centrifuged and dissolved in 20 mM Tris–HCl, 8 M Urea, pH 8.0 and frozen at −20°C until further use. For Aβ(1-42)-NT purification, cells were sonicated, centrifuged and filtered prior to loading to a HisPrep FF 16/10 column (GE Healthcare). Aβ(1-42)-NT was eluted in a 20 mM Tris–HCl, 8 M Urea, 300 mM Imidazole, pH 8.0 buffer, and cleaved with a TEV (tobacco etch virus) protease during dialysis in a 20 mM Tris–HCl, pH 8.0 buffer with 0.5 mM EDTA and 1.5 mM DTT at 4°C overnight. The cleaved Aβ(1-42) was purified on a HiLoad 16/600 Superdex 30 pg. (GE Healthcare) size exclusion column with a 20 mM sodium phosphate, pH 8.0 buffer. The Aβ(1-42) peptide was aliquoted, snap frozen, lyophilized and stored in −20°C until further use. Prior to all kinetics experiments and AFM imaging, lyophilized Aβ(1-42) was dissolved in 6 M guanidine hydrochloride for 20 min on ice before purification by size exclusion chromatography in a 20 mM

1469896x, 2026, 12, Downloaded from https://onlinelibrary.wiley.com/doi/10.1002/pro.70849 by Statens Beredning, Wiley Online Library on [20/11/2026]. See the Terms and Conditions (https://onlinelibrary.wiley.com/terms-and-conditions) on Wiley Online Library for rules of use; OA articles are governed by the applicable Creative Commons License

sodium phosphate buffer, pH 8.0 using a 10/300 Superdex 75 column (GE Healthcare). Monomeric Aβ(1-42) was eluted as a single peak at approximately 14 mL and the concentration was determined from the integrated peak area in the chromatogram ($\varepsilon_{280nm} = 1280$/M/cm), as previously reported by us (Halipi et al., 2024).

4.8 | Thioflavin-T (ThT) monitored aggregation kinetics

Samples containing 2 μM of monomeric Aβ(1-42) in 20 mM phosphate buffer, pH 8.0 (prepared as described above), 5 μM ThT, and indicated concentrations of EVs (particles/mL) were prepared on ice and distributed in triplicate to non-binding, transparent bottom, black half-area 96-well microplates (Corning) sealed with adhesive film to prevent evaporation. ThT emission was measured with bottom optics in a FluoStar OPTIMA fluorescence plate reader (BMG Labtech) and a 440 ± 10 nm and a 485 ± 10 nm bandpass filter for excitation and emission respectively. All ThT measurements were performed at 37°C and quiescent conditions. The aggregation kinetic parameters half time (t_{half}), lag time (t_{lag}), and growth time (t_{growth}) were extracted from the ThT fluorescence aggregation curves. t_{half} denotes the reaction time to reach 50% of the total fibrillar mass formation, t_{lag} corresponds to the reaction time at which 10% of the final fibril content is attained, and t_{growth} denotes the reaction time needed to increase the fibril content from 10% to 90% of the end-point maximum.

4.9 | Analysis and modeling of kinetic data

The acquired kinetic data were analyzed to determine the dominant mechanism of aggregation and extract rate constants. A multi-step secondary nucleation dominated model (Cohen et al., 2013) on the web-based tool AmyloFit (Meisl, Kirkegaard, et al., 2016) was used to fit the experimental kinetic data. Experimental data for Aβ(1-42) in buffer was fitted, enabling estimation of rate constants for elongation and primary nucleation or elongation and secondary nucleation; k_+k_n and k_+k_2, respectively. KM was determined and kept constant for further analysis. These values were used as initial guesses when analyzing Aβ(1-42) aggregation kinetics data in the presence of EVs. The same model, with initial guesses, was used to fit Aβ(1-42) aggregation data in the presence of EVs, yielding combined rate constants for elongation and primary nucleation or elongation and secondary nucleation; k_+k_n and k_+k_2, respectively. The goodness of fits was evaluated based on mean residual errors.

4.10 | Atomic force microscopy

Samples for atomic force microscopy (AFM) were prepared by depositing 10 μL of sample onto a freshly cleaved mica surface functionalized with 10 μL (3-aminopropyl)triethoxysilane for 30 s, washed with Milli Q water, and dried with nitrogen gas. Samples were incubated on the mica for 10 min to let fibrils attach and then the mica was washed with MQ followed by drying with nitrogen gas. All samples were stored in closed containers until imaging began. Recording of AFM images was performed using an NTEGRA system with a gold-covered crystal cantilever (NT-MDT, NSG01, force constant ~ 5.1 N/m, resonance frequency ~150 Hz). The 10 × 10 μm images with 256 × 256 pixels were recorded for all samples and images were analyzed using Gwyddion software by planar subtraction, polynomial background subtraction, correction of horizontal aberrations and minimum value shift to zero. One hundred Aβ(1-42) fibrils per sample were measured for fibril length and height based on 10–11 AFM images. The data were analyzed by performing a one-way ANOVA Post-hoc Bonferroni-corrected means comparison tests [OriginPro 2020 software (OriginLab)].

AUTHOR CONTRIBUTIONS

Vesa Halipi: Conceptualization; investigation; writing – original draft; methodology; validation; visualization; writing – review and editing; formal analysis; data curation. **Georgia Daoutsali:** Investigation; methodology; validation; formal analysis; data curation. **Fritjof Havemeister:** Formal analysis; data curation; investigation. **Viktoria de Carvalho:** Investigation. **André Görgens:** Writing – review and editing; resources. **Samir El Andaloussi:** Resources. **Elin K. Esbjörner:** Writing – original draft; funding acquisition; investigation; conceptualization; visualization; writing – review and editing; validation; supervision; resources; project administration; formal analysis.

ACKNOWLEDGMENTS

This work was funded by grants to E.K.E from the Swedish research council (2016-03902 and 2020-05303), the Knut and Alice Wallenberg foundation (2019.0238, 2022.0134) and the Swedish foundation for strategic research (SSF) funded FoRmulaEx research centre (IRC15-0065).

DATA AVAILABILITY STATEMENT

All data needed to evaluate the conclusions in the paper are present in the paper and/or the Supplementary

1469896x, 2026, 12, Downloaded from https://onlinelibrary.wiley.com/doi/10.1002/pro.70849 by Statens Beredning, Wiley Online Library on [20/11/2026]. See the Terms and Conditions (https://onlinelibrary.wiley.com/terms-and-conditions) on Wiley Online Library for rules of use; OA articles are governed by the applicable Creative Commons License

Information. Raw data supporting the findings of this manuscript are available from the corresponding author upon request.

ORCID

Vesa Halipi https://orcid.org/0000-0002-9921-0483
André Görgens https://orcid.org/0000-0001-9198-0857
Elin K. Esbjörner https://orcid.org/0000-0002-1253-6342

REFERENCES

Abelein A, Chen G, Kitoka K, Aleksis R, Oleskovs F, Sarr M, et al. High-yield production of amyloid-beta peptide enabled by a customized spider silk domain. Sci Rep. 2020;10:235.

Abels ER, Breakefield XO. Introduction to extracellular vesicles: biogenesis, RNA Cargo selection, content, release, and uptake. Cell Mol Neurobiol. 2016;36:301–12.

Agholme L, Lindstrom T, Kagedal K, Marcusson J, Hallbeck M. An in vitro model for neuroscience: differentiation of SH-SY5Y cells into cells with morphological and biochemical characteristics of mature neurons. J Alzheimer's Dis. 2010;20:1069–82.

Amand HL, Rydberg HA, Fornander LH, Lincoln P, Norden B, Esbjorner EK. Cell surface binding and uptake of arginine- and lysine-rich penetratin peptides in absence and presence of proteoglycans. Biochim Biophys Acta. 2012;1818:2669–78.

Amaro M, Sachl R, Aydogan G, Mikhalyov II, Vacha R, Hof M. GM1 ganglioside inhibits beta-amyloid oligomerization induced by sphingomyelin. Angew Chem Int Ed Engl. 2016;55:9411–5.

Amin S, Massoumi H, Tewari D, Roy A, Chaudhuri M, Jazayerli C, et al. 'Cell type-specific extracellular vesicles and their impact on health and disease. Int J Mol Sci. 2024;25:2730.

Ariga T, McDonald MP, Yu RK. Role of ganglioside metabolism in the pathogenesis of Alzheimer's disease—a review. J Lipid Res. 2008;49:1157–75.

Banerjee S, Hashemi M, Zagorski K, Lyubchenko YL. Cholesterol in membranes facilitates aggregation of amyloid beta protein at physiologically relevant concentrations. ACS Chem Nerosci. 2021;12:506–16.

Basso M, Bonetto V. Extracellular vesicles and a novel form of communication in the brain. Front Neurosci. 2016;10:127.

Baumann KN, Sneideriene G, Sanguanini M, Schneider M, Rimon O, Gonzalez Diaz A, et al. A kinetic map of the influence of biomimetic lipid model membranes on Abeta(42) aggregation. ACS Chem Neurosci. 2023;14:323–9.

Bolognesi B, Cohen SI, Aran Terol P, Esbjorner EK, Giorgetti S, Mossuto MF, et al. Single point mutations induce a switch in the molecular mechanism of the aggregation of the Alzheimer's disease associated Abeta42 peptide. ACS Chem Biol. 2014;9:378–82.

Calamai M, Pavone FS. Partitioning and confinement of GM1 ganglioside induced by amyloid aggregates. FEBS Lett. 2013;587:1385–91.

Cerezo-Magana M, Bang-Rudenstam A, Belting M. The pleiotropic role of proteoglycans in extracellular vesicle mediated communication in the tumor microenvironment. Semin Cancer Biol. 2020;62:99–107.

Choi D, Go G, Kim DK, Lee J, Park SM, Di Vizio D, et al. Quantitative proteomic analysis of trypsin-treated extracellular vesicles to identify the real-vesicular proteins. J Extracell Vesicles. 2020;9:1757209.

Christianson HC, Svensson KJ, van Kuppevelt TH, Li JP, Belting M. Cancer cell exosomes depend on cell-surface heparan sulfate proteoglycans for their internalization and functional activity. Proc Natl Acad Sci U S A. 2013;110:17380–5.

Cohen SI, Linse S, Luheshi LM, Hellstrand E, White DA, Rajah L, et al. Proliferation of amyloid-beta42 aggregates occurs through a secondary nucleation mechanism. Proc Natl Acad Sci U S A. 2013;110:9758–63.

Cohen SIA, Arosio P, Presto J, Kurudenkandy FR, Biverstal H, Dolfe L, et al. A molecular chaperone breaks the catalytic cycle that generates toxic Abeta oligomers. Nat Struct Mol Biol. 2015;22:207–13.

Corso G, Mager I, Lee Y, Gorgens A, Bultema J, Giebel B, et al. Reproducible and scalable purification of extracellular vesicles using combined bind-elute and size exclusion chromatography. Sci Rep. 2017;7:11561.

Da Conceicao ARR, Marinatto J, Pinheiro LS, Rody T, De Felice FG. The multifaceted role of extracellular vesicles in Alzheimer's disease. J Neurochem. 2025;169:e70209.

Di Paolo G, Kim TW. Linking lipids to Alzheimer's disease: cholesterol and beyond. Nat Rev Neurosci. 2011;12:284–96.

Elia CA, Tamborini M, Rasile M, Desiato G, Marchetti S, Swuec P, et al. Intracerebral injection of extracellular vesicles from mesenchymal stem cells exerts reduced Abeta plaque burden in early stages of a preclinical model of Alzheimer's disease. Cells. 2019;8:1059.

Esko JD, Stewart TE, Taylor WH. Animal cell mutants defective in glycosaminoglycan biosynthesis. Proc Natl Acad Sci U S A. 1985;82:3197–201.

Gabrielli M, Prada I, Joshi P, Falcicchia C, D'Arrigo G, Rutigliano G, et al. Microglial large extracellular vesicles propagate early synaptic dysfunction in Alzheimer's disease. Brain. 2022;145:2849–68.

Ghadami S, Dellinger K. The lipid composition of extracellular vesicles: applications in diagnostics and therapeutic delivery. Front Mol Biosci. 2023;10:1198044.

Gorgens A, Corso G, Hagey DW, Jawad Wiklander R, Gustafsson MO, Felldin U, et al. Identification of storage conditions stabilizing extracellular vesicles preparations. J Extracell Vesicles. 2022;11:e12238.

Gouras GK, Tsai J, Naslund J, Vincent B, Edgar M, Checler F, et al. Intraneuronal Abeta42 accumulation in human brain. Am J Pathol. 2000;156:15–20.

Gravina SA, Ho L, Eckman CB, Long KE, Otvos L Jr, Younkin LH, et al. Amyloid beta protein (a beta) in Alzheimer's disease brain. Biochemical and immunocytochemical analysis with antibodies specific for forms ending at a beta 40 or a beta 42(43). J Biol Chem. 1995;270:7013–6.

Haass C, Selkoe DJ. Soluble protein oligomers in neurodegeneration: lessons from the Alzheimer's amyloid beta-peptide. Nat Rev Mol Cell Biol. 2007;8:101–12.

Habchi J, Chia S, Galvagnion C, Michaels TCT, Bellaiche MMJ, Ruggeri FS, et al. Cholesterol catalyses Abeta42 aggregation through a heterogeneous nucleation pathway in the presence of lipid membranes. Nat Chem. 2018;10:673–83.

Hagey DW, Ojansivu M, Bostancioglu BR, Saher O, Bost JP, Gustafsson MO, et al. The cellular response to extracellular vesicles is dependent on their cell source and dose. Sci Adv. 2023;9:eadh1168.

Halipi V, Sasanian N, Feng J, Hu J, Lubart Q, Bernson D, et al. Extracellular vesicles slow down aβ(1-42) aggregation by interfering with the amyloid fibril elongation step. ACS Chem Neurosci. 2024;15:944–54.

Hallal S, Tuzesi A, Grau GE, Buckland ME, Alexander KL. Understanding the extracellular vesicle surface for clinical molecular biology. J Extracell Vesicles. 2022;11:e12260.

Hampel H, Hardy J, Blennow K, Chen C, Perry G, Kim SH, et al. The amyloid-beta pathway in Alzheimer's disease. Mol Psychiatry. 2021;26:5481–503.

He X, Guan F, Lei L. Structure and function of glycosphingolipids on small extracellular vesicles. Glycoconj J. 2022;39:197–205.

1469896x, 2026, 12, Downloaded from https://onlinelibrary.wiley.com/doi/10.1002/pro.70849 by Statens Beredning, Wiley Online Library on [20/11/2026]. See the Terms and Conditions (https://onlinelibrary.wiley.com/terms-and-conditions) on Wiley Online Library for rules of use; OA articles are governed by the applicable Creative Commons License

Hill AF. Extracellular vesicles and neurodegenerative diseases. J Neurosci. 2019;39:9269–73.
Jan A, Adolfsson O, Allaman I, Buccarello AL, Magistretti PJ, Pfeifer A, et al. Abeta42 neurotoxicity is mediated by ongoing nucleated polymerization process rather than by discrete Abeta42 species. J Biol Chem. 2011;286:8585–96.
Jarrett JT, Berger EP, Lansbury PT Jr. The carboxy terminus of the beta amyloid protein is critical for the seeding of amyloid formation: implications for the pathogenesis of Alzheimer's disease. Biochemistry. 1993;32:4693–7.
Jeppesen DK, Nawrocki A, Jensen SG, Thorsen K, Whitehead B, Howard KA, et al. Quantitative proteomics of fractionated membrane and lumen exosome proteins from isogenic metastatic and nonmetastatic bladder cancer cells reveal differential expression of EMT factors. Proteomics. 2014;14:699–712.
Jia Y, Yu L, Ma T, Xu W, Qian H, Sun Y, et al. Small extracellular vesicles isolation and separation: Current techniques, pending questions and clinical applications. Theranostics. 2022;12:6548–75.
Lakowicz JR. Principles of frequency-domain fluorescence spectroscopy and applications to cell membranes. Subcell Biochem. 1988;13:89–126.
Laulagnier K, Motta C, Hamdi S, Roy S, Fauvelle F, Pageaux JF, et al. Mast cell- and dendritic cell-derived exosomes display a specific lipid composition and an unusual membrane organization. Biochem J. 2004;380:161–71.
Lindberg DJ, Wesen E, Bjorkeroth J, Rocha S, Esbjorner EK. Lipid membranes catalyse the fibril formation of the amyloid-beta (1-42) peptide through lipid-fibril interactions that reinforce secondary pathways. Biochim Biophys Acta Biomembr. 2017;1859:1921–9.
Linse S, Scheidt T, Bernfur K, Vendruscolo M, Dobson CM, Cohen SIA, et al. Kinetic fingerprints differentiate the mechanisms of action of anti-Abeta antibodies. Nat Struct Mol Biol. 2020;27:1125–33.
Losurdo M, Pedrazzoli M, D'Agostino C, Elia CA, Massenzio F, Lonati E, et al. Intranasal delivery of mesenchymal stem cell-derived extracellular vesicles exerts immunomodulatory and neuroprotective effects in a 3xTg model of Alzheimer's disease. Stem Cells Transl Med. 2020;9:1068–84.
Lue LF, Kuo YM, Roher AE, Brachova L, Shen Y, Sue L, et al. Soluble amyloid beta peptide concentration as a predictor of synaptic change in Alzheimer's disease. Am J Pathol. 1999;155:853–62.
McGeer PL, Itagaki S, Tago H, McGeer EG. Reactive microglia in patients with senile dementia of the Alzheimer type are positive for the histocompatibility glycoprotein HLA-DR. Neurosci Lett. 1987;79:195–200.
Meisl G, Kirkegaard JB, Arosio P, Michaels TCT, Vendruscolo M, Dobson CM, et al. Molecular mechanisms of protein aggregation from global fitting of kinetic models. Nat Protoc. 2016;11:252–72.
Meisl G, Yang X, Frohm B, Knowles TP, Linse S. Quantitative analysis of intrinsic and extrinsic factors in the aggregation mechanism of Alzheimer-associated Abeta-peptide. Sci Rep. 2016;6:18728.
Meisl G, Yang X, Hellstrand E, Frohm B, Kirkegaard JB, Cohen SI, et al. Differences in nucleation behavior underlie the contrasting aggregation kinetics of the Abeta40 and Abeta42 peptides. Proc Natl Acad Sci U S A. 2014;111:9384–9.
Minter MR, Taylor JM, Crack PJ. The contribution of neuroinflammation to amyloid toxicity in Alzheimer's disease. J Neurochem. 2016;136:457–74.
Munke A, Persson J, Weiffert T, De Genst E, Meisl G, Arosio P, et al. Phage display and kinetic selection of antibodies that specifically inhibit amyloid self-replication. Proc Natl Acad Sci U S A. 2017;114:6444–9.
Osteikoetxea X, Balogh A, Szabo-Taylor K, Nemeth A, Szabo TG, Paloczi K, et al. Improved characterization of EV preparations based on protein to lipid ratio and lipid properties. PLoS One. 2015;10:e0121184.
Owen MC, Kulig W, Poojari C, Rog T, Strodel B. Physiologically-relevant levels of sphingomyelin, but not GM1, induces a beta-sheet-rich structure in the amyloid-beta(1-42) monomer. Biochim Biophys Acta Biomembr. 2018;1860:1709–20.
Pait MC, Kaye SD, Su Y, Kumar A, Singh S, Gironda SC, et al. Novel method for collecting hippocampal interstitial fluid extracellular vesicles (EV(ISF)) reveals sex-dependent changes in microglial EV proteome in response to Abeta pathology. J Extracell Vesicles. 2024;13:e12398.
Parolini I, Federici C, Raggi C, Lugini L, Palleschi S, De Milito A, et al. Microenvironmental pH is a key factor for exosome traffic in tumor cells. J Biol Chem. 2009;284:34211–22.
Radko SP, Khmeleva SA, Mantsyzov AB, Kiseleva YY, Mitkevich VA, Kozin SA, et al. Heparin modulates the kinetics of zinc-induced aggregation of amyloid-beta peptides. J Alzheimers Dis. 2018;63:539–50.
Rajendran L, Honsho M, Zahn TR, Keller P, Geiger KD, Verkade P, et al. Alzheimer's disease beta-amyloid peptides are released in association with exosomes. Proc Natl Acad Sci U S A. 2006;103:11172–7.
Sandwall E, O'Callaghan P, Zhang X, Lindahl U, Lannfelt L, Li JP. Heparan sulfate mediates amyloid-beta internalization and cytotoxicity. Glycobiology. 2010;20:533–41.
Sanguanini M, Baumann KN, Preet S, Chia S, Habchi J, Knowles TPJ, et al. Complexity in lipid membrane composition induces resilience to Abeta(42) aggregation. ACS Chem Neurosci. 2020;11:1347–52.
Sasanian N, Halipi V, Sjogren M, Bengtsson J, Bernson D, Esbjorner EK. Ganglioside GM1 slows down Abeta(1-42) aggregation by a primary nucleation inhibitory mechanism that is modulated by sphingomyelin and cholesterol. Commun Chem. 2025;9:39.
Scheltens P, De Strooper B, Kivipelto M, Holstege H, Chetelat G, Teunissen CE, et al. Alzheimer's disease. Lancet. 2021;397:1577–90.
Selkoe DJ, Hardy J. The amyloid hypothesis of Alzheimer's disease at 25 years. EMBO Mol Med. 2016;8:595–608.
Shtam T, Naryzhny S, Kopylov A, Petrenko E, Samsonov R, Kamyshinsky R, et al. Functional properties of circulating exosomes mediated by surface-attached plasma proteins. J Hematol. 2018;7:149–53.
Silva RO, Haddad M, Counil H, Zaouter C, Patten SA, Fulop T, et al. Exploring the potential of plasma and adipose mesenchymal stem cell-derived extracellular vesicles as novel platforms for neuroinflammation therapy. J Control Release. 2025;377:880–98.
Skliar M, Chernyshev VS, Belnap DM, Sergey GV, Al-Hakami SM, Bernard PS, et al. Membrane proteins significantly restrict exosome mobility. Biochem Biophys Res Commun. 2018;501:1055–9.
Skotland T, Sagini K, Sandvig K, Llorente A. An emerging focus on lipids in extracellular vesicles. Adv Drug Deliv Rev. 2020;159:308–21.
Snow AD, Mar H, Nochlin D, Sekiguchi RT, Kimata K, Koike Y, et al. Early accumulation of heparan sulfate in neurons and in the beta-amyloid protein-containing lesions of Alzheimer's disease and Down's syndrome. Am J Pathol. 1990;137:1253–70.
Snow AD, Sekiguchi RT, Nochlin D, Kalaria RN, Kimata K. Heparan sulfate proteoglycan in diffuse plaques of hippocampus but not of cerebellum in Alzheimer's disease brain. Am J Pathol. 1994;144:337–47.
Sokolow S, Henkins KM, Bilousova T, Miller CA, Vinters HV, Poon W, et al. AD synapses contain abundant Abeta monomer and multiple soluble oligomers, including a 56-kDa assembly. Neurobiol Aging. 2012;33:1545–55.
Takahashi RH, Nagao T, Gouras GK. Plaque formation and the intraneuronal accumulation of beta-amyloid in Alzheimer's disease. Pathol Int. 2017;67:185–93.

1469896x, 2026, 12, Downloaded from https://onlinelibrary.wiley.com/doi/10.1002/pro.70049 by Statens Beredning, Wiley Online Library on [20/11/2026]. See the Terms and Conditions (https://onlinelibrary.wiley.com/terms-and-conditions) on Wiley Online Library for rules of use; OA articles are governed by the applicable Creative Commons License

Tiwari S, Atluri V, Kaushik A, Yndart A, Nair M. Alzheimer's disease: pathogenesis, diagnostics, and therapeutics. Int J Nanomed. 2019;14:5541–54.

Udan ML, Ajit D, Crouse NR, Nichols MR. Toll-like receptors 2 and 4 mediate Abeta(1-42) activation of the innate immune response in a human monocytic cell line. J Neurochem. 2008;104:524–33.

van Dyck CH, Swanson CJ, Aisen P, Bateman RJ, Chen C, Gee M, et al. Lecanemab in early Alzheimer's disease. New England J Med. 2023;388:9–21.

van Horssen J, Wesseling P, van den Heuvel LP, de Waal RM, Verbeek MM. Heparan sulphate proteoglycans in Alzheimer's disease and amyloid-related disorders. Lancet Neurol. 2003;2:482–92.

van Niel G, D'Angelo G, Raposo G. Shedding light on the cell biology of extracellular vesicles. Nat Rev Mol Cell Biol. 2018;19:213–28.

Vandendriessche C, Bruggeman A, Van Cauwenberghe C, Vandenbroucke RE. Extracellular vesicles in Alzheimer's and Parkinson's disease: small entities with large consequences. Cells. 2020;9:2485.

Vingtdeux V, Sergeant N, Buee L. Potential contribution of exosomes to the prion-like propagation of lesions in Alzheimer's disease. Front Physiol. 2012;3:229.

Wang J, Xing K, Zhang G, Li Z, Ding X, Leong DT. Surface components and biological interactions of extracellular vesicles. ACS Nano. 2025;19:8433–61.

Wang X, Yang G. Bone marrow mesenchymal stem cells-derived exosomes reduce Abeta deposition and improve cognitive function recovery in mice with Alzheimer's disease by activating sphingosine kinase/sphingosine-1-phosphate signaling pathway. Cell Biol Int. 2021;45:775–84.

Welsh JA, Goberdhan DCI, O'Driscoll L, Buzas EI, Blenkiron C, Bussolati B, et al. Minimal information for studies of extracellular vesicles (MISEV2023): from basic to advanced approaches. J Extracell Vesicles. 2024;13:e12404.

Wesen E, Gallud A, Paul A, Lindberg DJ, Malmberg P, Esbjorner EK. Cell surface proteoglycan-mediated uptake and accumulation of the Alzheimer's disease peptide Abeta(1-42). Biochim Biophys Acta Biomembr. 2018;1860:2204–14.

Williams C, Royo F, Aizpurua-Olaizola O, Pazos R, Boons GJ, Reichardt NC, et al. Glycosylation of extracellular vesicles: current knowledge, tools and clinical perspectives. J Extracell Vesicles. 2018;7:1442985.

Xicoy H, Wieringa B, Martens GJ. The SH-SY5Y cell line in Parkinson's disease research: a systematic review. Mol Neurodegener. 2017;12:10.

Xue WF, Hellewell AL, Gosal WS, Homans SW, Hewitt EW, Radford SE. Fibril fragmentation enhances amyloid cytotoxicity. J Biol Chem. 2009;284:34272–82.

Yanagisawa K, Odaka A, Suzuki N, Ihara Y. GM1 ganglioside-bound amyloid beta-protein (A beta): a possible form of preamyloid in Alzheimer's disease. Nat Med. 1995;1:1062–6.

Yanez-Mo M, Siljander PR, Andreu Z, Zavec AB, Borras FE, Buzas EI, et al. Biological properties of extracellular vesicles and their physiological functions. J Extracell Vesicles. 2015;4:27066.

Yuyama K, Sun H, Sakai S, Mitsutake S, Okada M, Tahara H, et al. Decreased amyloid-beta pathologies by intracerebral loading of glycosphingolipid-enriched exosomes in Alzheimer model mice. J Biol Chem. 2014;289:24488–98.

Zhang X, Wesen E, Kumar R, Bernson D, Gallud A, Paul A, et al. Correlation between cellular uptake and cytotoxicity of fragmented alpha-Synuclein amyloid fibrils suggests intracellular basis for toxicity. ACS Chem Nerosci. 2020;11:233–41.

Zhang Y, Chen H, Li R, Sterling K, Song W. Amyloid beta-based therapy for Alzheimer's disease: challenges, successes and future. Signal Transduct Target Ther. 2023;8:248.

SUPPORTING INFORMATION

Additional supporting information can be found online in the Supporting Information section at the end of this article.

How to cite this article: Halipi V, Daoutsali G, Havemeister F, de Carvalho V, Görgens A, El Andaloussi S, et al. Surface proteins modulate extracellular vesicle mediated inhibition of Aβ(1-42) aggregation. Protein Science. 2026;35(12):e70849. https://doi.org/10.1002/pro.70849

1469896x, 2026, 12, Downloaded from https://onlinelibrary.wiley.com/doi/10.1002/pro.70849 by Statens Beredning, Wiley Online Library on [20/11/2026]. See the Terms and Conditions (https://onlinelibrary.wiley.com/terms-and-conditions) on Wiley Online Library for rules of use; OA articles are governed by the applicable Creative Commons License